Strong angular magneto-induced anisotropy of Voigt effect in metal-dielectric metamaterials with periodic nanostructures

Yakov M. Strelniker[1,*] and David J. Bergman[2,†]

[1]*Department of Physics, Bar-Ilan University, IL-52900 Ramat-Gan, Israel*

[2]*Raymond and Beverly Sackler School of Physics and Astronomy, Faculty of Exact Sciences, Tel Aviv University, IL-69978 Tel Aviv, Israel*

(Received 12 November 2013; revised manuscript received 10 March 2014; published 31 March 2014)

When an applied magnetic field has an arbitrary direction with respect to the lattice axes of a periodically microstructured or nanostructured metamaterial, the effective permittivity tensor of the metamaterial sample becomes anisotropic and all its components can be nonzero. This is true even if the microstructure has a high symmetry, e.g., cubic or triangular. It is found that the strong magneto-induced anisotropy which appears in the macroscopic response leads to an unusually strong anisotropic behavior of the Voigt effect and other magneto-optical effects. That is, these phenomena become strongly dependent on the direction of the applied static magnetic field, as well as on the direction of the time-dependent electromagnetic field, with respect to the symmetry axes of the periodic microstructure.

DOI: 10.1103/PhysRevB.89.125312 PACS number(s): 78.66.Sq, 78.20.Ls, 73.20.Mf, 78.67.−n

I. INTRODUCTION

It is well known that natural or artificial materials with cubic or square lattices exhibit absolutely isotropic transport and optical, thermoelectrical, and other properties. Recently, we have shown that application of a strong-enough magnetic field $\mathbf{B}_0$ can spoil this isotropy when the cubic or square array of insulating (conducting) inclusions are placed inside a conducting (insulating) host medium (i.e., in the case of periodical composites or, as they are now called, metamaterials) [1–4]. Such a strong magneto-induced anisotropy can be observed when the dimensionless magnetic field $H = \mu_H|\mathbf{B}_0| = \omega_c\tau$ [where $\mathbf{B}_0$ is the applied magnetic field measured in conventional units, μ_H is the Hall mobility, ω_c is the cyclotron frequency, and τ is the conductivity relaxation time; see text following Eq. (58)] times the radius of the circular (or spherical) inclusion R is larger than the lattice constant a: $H \cdot R > a$. In Ref. [1] it was predicted that the strong field dc effective magnetoresistance $\hat{\rho}_e(H) = 1/\hat{\sigma}_e(H)$ (where $\hat{\sigma}_e$ is the macroscopic or bulk effective conductivity) of such metamaterials will exhibit a strong dependence on the precise orientations of the external magnetic field $\mathbf{B}_0$ (with respect to the main crystal lattice axes) and the volume-averaged current density $\langle\mathbf{J}\rangle$, very similar to its behavior in certain metallic single crystals; see Fig. 14 in Ref. [1]. Since $\hat{\sigma}_e$ can be measured directly, our predictions for $\hat{\sigma}_e(H)$ were already verified experimentally [5,6]. A similar magneto-induced anisotropy should exist in the case of ac conductivity, i.e., for the macroscopic or bulk effective permittivity tensor $\hat{\varepsilon}_e$ of metal-dielectric metamaterials and consequently for their optical properties [3,4]. However, since $\hat{\varepsilon}_e$ cannot be measured directly, our prediction for $\hat{\varepsilon}_e(H)$ has not yet been tested experimentally. What can be measured directly is the Faraday-like rotation. However, for the case of an in-plane magnetic field $\mathbf{B}_0$ in a metamaterial the relevant effect is Voigt rotation, for which general exact analytical expressions (as far as we know) are not published. In this paper we derive such exact expressions for the general case and verify our predictions numerically.

When a static magnetic field $\mathbf{B}_0$ is present the electric permittivity ceases to be a scalar quantity, even in a material that is homogeneous and isotropic. In the case of a dielectric material, the off-diagonal antisymmetric elements of the electric permittivity tensor $\hat{\varepsilon}$ result in the appearance of new macroscopic electromagnetic (EM) phenomena such as the Faraday and Voigt effects. The Faraday effect appears when a plane wave propagates in the direction of $\mathbf{B}_0$. In that case there are two normal modes of propagation with oppositely oriented circular polarizations and different phase velocities. Therefore, when the incident plane wave is plane polarized the polarization plane rotates as the wave advances. The Voigt effect (also known as the Cotton-Mouton effect) appears when $\mathbf{B}_0$ is perpendicular to the $\mathbf{k}$ vector of the plane wave. In this case, the normal propagating modes are elliptically polarized; again there are two of them and they have different phase velocities. Both the orientation of the polarization ellipses and their ellipticities, as well as the phase velocities, depend upon the elements of $\hat{\varepsilon}$.

It is well known that the Voigt, Faraday, and other magneto-optical (MO) effects can be significantly enhanced in the vicinity of an EM resonance [7,8]. One such resonance, which is currently under intensive study, is the surface plasma resonance. It is widely believed that this or similar resonances are responsible for the extraordinary light transmission (ELT) through a metal film, perforated by a periodic array of subwavelength holes [9]. Application of a static magnetic field $\mathbf{B}_0$ to such systems (see Fig. 1) induces strong optical and transport anisotropy and leads to the appearance of additional off-diagonal tensor components in the macroscopic permittivity tensor $\hat{\varepsilon}_e$ (see Fig. 2) and changes the frequency of the surface plasma resonance [3,4,10]. Therefore, the application of a static magnetic field to a conducting system with dielectric islands or to a dielectric system with metallic islands should lead to the appearance of strong MO effects and to possibilities for the manipulation of light propagation. This was shown both theoretically [3,4,11,12] and experimentally [13–15].

*strelnik@mail.biu.ac.il

†bergman@post.tau.ac.il

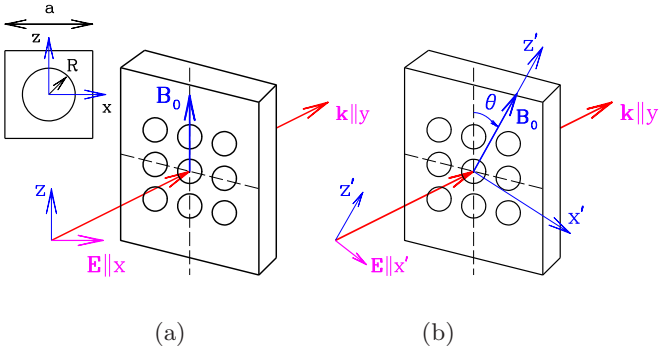

FIG. 1. (Color online) (a) Schematic drawing of a metal film with a periodic array of holes. The fixed coordinate axes x,z are always directed along the principal axes of the simple-square lattice of holes and the applied static magnetic field $\mathbf{B}_0$ lies in the film plane. The incident light beam is normal to the film surface; i.e., the ac electric field $\mathbf{E}$ is parallel to the film plane, while the wave vector is normal to it (i.e., $\mathbf{k} \parallel y$). Note that the ac magnetic field $\mathbf{H}$ of the light wave ($\mathbf{H} \perp \mathbf{E}$) is not important in our considerations and we omit it everywhere. (Inset) The $a \times a$ unit cell of the simple-square periodic composite film with a cylindrical hole of radius R at its center. (b) The same as (a) but both $\mathbf{B}_0$ and the incident field $\mathbf{E}$ are rotated in the film plane. The x' and z' axes are referred to in the text as the "rotating coordinates."

After the phenomenon of ELT in the presence of applied static magnetic field was discussed in Refs. [4,11], several attempts were made to consider different MO effects in the case of light propagating through a perforated metallic film [16–22] or a film with metallic islands [23–29]. However, in most of these studies only the Faraday configuration was considered, where the magnetic field $\mathbf{B}_0$ is normal to the film plane. In very few of them [30] was the Voigt configuration (i.e., where the magnetic field is applied parallel to the film plane) considered. From intuitive physical considerations we expect that when an in-plane magnetic field is rotated with respect to the main axes of the microstructure, a magneto-induced angular anisotropy of the different MO effects will be observed. In this paper we consider the general case of arbitrary orientation of the magnetic field with respect to the film microstructure.

In the case where $\mathbf{B}_0$ has an arbitrary direction with respect to the lattice axes of the microstructure, all components of the permittivity tensor can be nonzero [3,4,11]. When both the external magnetic field $\mathbf{B}_0$ and the EM electric field $\mathbf{E}$ are rotated in the film plane, the angular profiles of all the permittivity tensor components are quite complicated (see Refs. [3,4,11] and Fig. 2). As a result of this, the general expressions for Faraday rotation and Voigt effect are also quite complicated. Therefore, the MO effects in metamaterial crystals need to be calculated using appropriate general expressions, where simplistic assumptions regarding the form of $\hat{\varepsilon}_e$ are avoided.

The remainder of this paper is arranged as follows. In Sec. II, we derive the dispersion relation of the light propagating through the metamaterial in the presence of an arbitrarily directed external magnetic field $\mathbf{B}_0$. In Sec. III we generalize results of Ref. [31] and find the electric field components $\mathbf{E}$ of the light beam propagating through the metamaterial film

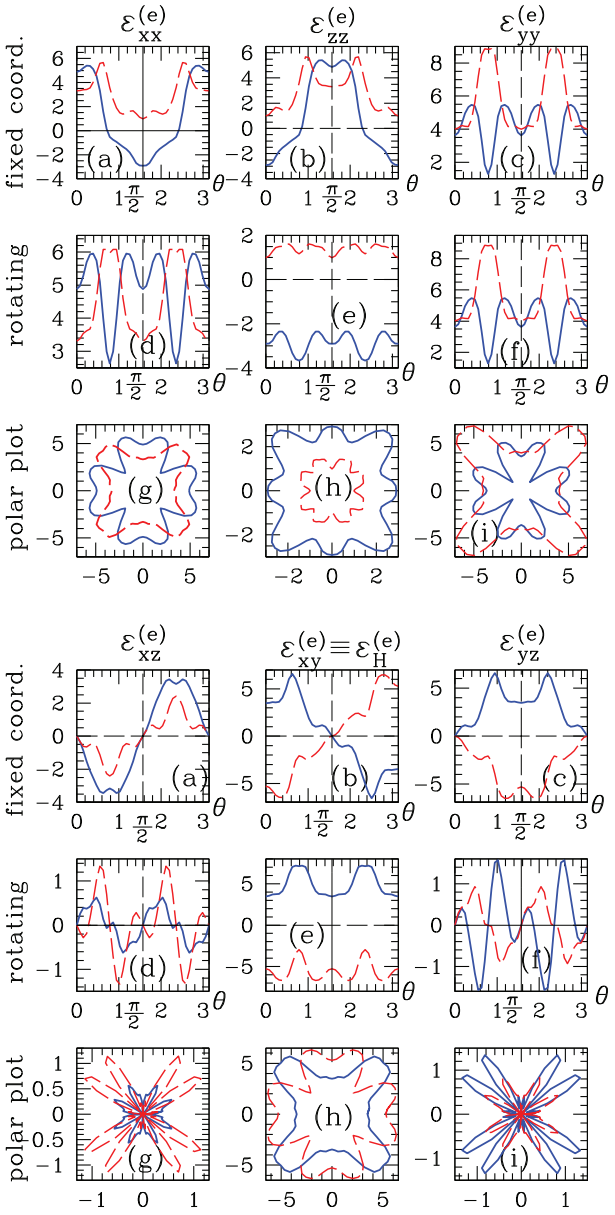

FIG. 2. (Color online) Real (solid blue lines) and imaginary (dashed red lines) parts of the diagonal (top part) and off-diagonal (lower part) components of the macroscopic permittivity tensor $\hat{\varepsilon}_e$ of the metamaterial, made of a simple-square array (with lattice constant a) of circular cylinder holes (of radius $R = 0.3a$) in a metal film. In the top half, panels (a)–(c) exhibit this in the fixed coordinate system, plotted vs the rotation angle θ (in radians) of Fig. 1(b). Panels (d)–(f) exhibit this in the *rotating* coordinates of Fig. 1(b). Panels (g)–(i) are polar plots of the absolute values of the same results shown in (d)–(f). In the bottom half, the $\varepsilon^{(e)}_{xy}$ component of the permittivity tensor $\hat{\varepsilon}_e$ is the Hall component $\varepsilon^{(e)}_H$. For any orientation of $\mathbf{B}_0$ in the x,z plane (i.e., $B_{0y} = 0$) the following symmetry relations hold: $\varepsilon^{(e)}_{xz} = \varepsilon^{(e)}_{zx}$, $\varepsilon^{(e)}_{yz} = -\varepsilon^{(e)}_{zy}$. The permittivity tensor is taken (in both top and lower parts) in the quasistatic approximation $\hat{\varepsilon} = \hat{\varepsilon}_0 + i4\pi\hat{\sigma}/\omega$, where $\hat{\sigma}$ is the Drude conductivity tensor [see Eq. (13) of Ref. [1] for the Drude conductivity tensor $\hat{\sigma}$ with arbitrary direction of $\mathbf{B}_0$] where the plasma frequency ω_p and the conductivity relaxation time τ are such that $\omega_p\tau = 20$. The light frequency is $\omega = 0.4\omega_p$ and the dimensionless magnetic field $H = 10$; see text after Eq. (58) for the definition of H.

in the presence of such an external magnetic field. In Sec. IV we find the polarization rotation and ellipticity in the general case. In Sec. V we give a brief presentation of our calculational scheme. In Sec. VI, we present our numerical results, followed by a brief discussion in Sec. VII. In Appendix A, we obtain some expressions for rotation and ellipticity in the case of arbitrary direction of $\mathbf{B}_0$ using the expressions for the EM field propagating through the sample (derived in Sec. II). This can be done using direct consideration of the ellipse of polarization, as well as by means of the Stokes parameters. For convenience, some general textbook material for these evaluations is summarized in Appendix B.

II. DISPERSION RELATION OF LIGHT IN A METAMATERIAL IN THE PRESENCE OF AN EXTERNAL STATIC MAGNETIC FIELD

We consider a metal film with an array of perpendicular holes, which is placed in a static, in-plane magnetic field $\mathbf{B}_0$ with an otherwise arbitrary direction. We characterize this part of our system by an effective permittivity tensor $\hat{\varepsilon}_e$, which we calculate following our previous works [3,4,32–34]. The second part of our system is a monochromatic light beam, of angular frequency ω, which impinges upon this film along the perpendicular axis y with linear polarization along the principal axis x of the array; see Fig. 1. We seek a solution of Maxwell's equations in the form of a monochromatic plane wave with frequency ω propagating along the y axis, with electric and magnetic fields $\mathbf{E} = \mathbf{E}_0 e^{i\omega t - i\mathbf{k}\cdot\mathbf{r}}$ and $\mathbf{H} = \mathbf{H}_0 e^{i\omega t - i\mathbf{k}\cdot\mathbf{r}}$. Here $\mathbf{E}_0$ and $\mathbf{H}_0$ are constant amplitudes and $\mathbf{k} \equiv (0,k,0)$ is the wave vector in the y direction. Substituting this in the macroscopic Maxwell equations we obtain a dispersion equation for the complex wave vector $\mathbf{k}$ [35–41],

$$k^2\mathbf{E}_0 - \mathbf{k}(\mathbf{E}_0\cdot\mathbf{k}) = \frac{\omega^2}{c^2}\hat{\varepsilon}_e(\omega)\cdot\mathbf{E}_0, \tag{1}$$

where $\hat{\varepsilon}_e(\omega)$ is the macroscopic or bulk effective electric permittivity tensor of the considered metamaterial, and $\mathbf{k} \equiv \frac{\omega}{c}N\mathbf{k}_0 \equiv \frac{\omega}{c}(n' + in'')\mathbf{k}_0$, where $\mathbf{k}_0$ is a real unit vector in the direction of $\mathbf{k}$ and $N \equiv n' + in''$ is the *complex* refractive index. The real part, n', determines the phase velocity, $v_p = c/n'$, and the imaginary part, n'', is the *absorption index* (or the *extinction* coefficient).

For the vector directions shown in Fig. 1, where the x and z axes are in the film plane and the light propagates along the y axis, Eq. (1) is easily seen to lead to

$$E_y = -\frac{\varepsilon_{yx}^{(e)}}{\varepsilon_{yy}^{(e)}}E_x - \frac{\varepsilon_{yz}^{(e)}}{\varepsilon_{yy}^{(e)}}E_z, \tag{2}$$

$$0 = \left[\left(\frac{c}{\omega}\right)^2 k^2 - \varepsilon_{xx}^{(e)} + \frac{\varepsilon_{xy}^{(e)}\varepsilon_{yx}^{(e)}}{\varepsilon_{yy}^{(e)}}\right]E_x - \left(\varepsilon_{xz}^{(e)} - \frac{\varepsilon_{xy}^{(e)}\varepsilon_{yz}^{(e)}}{\varepsilon_{yy}^{(e)}}\right)E_z, \tag{3}$$

$$0 = \left(\varepsilon_{zx}^{(e)} - \frac{\varepsilon_{zy}^{(e)}\varepsilon_{yx}^{(e)}}{\varepsilon_{yy}^{(e)}}\right)E_x - \left[\left(\frac{c}{\omega}\right)^2 k^2 - \varepsilon_{zz}^{(e)} + \frac{\varepsilon_{zy}^{(e)}\varepsilon_{yz}^{(e)}}{\varepsilon_{yy}^{(e)}}\right]E_z. \tag{4}$$

The homogeneous Eqs. (3) and (4) have a nontrivial solution only if their 2×2 determinant vanishes. This requirement leads to a dispersion equation for the wave numbers $k_\pm$, which are complex in general, as functions of the real angular frequency ω, where the subscript $\pm$ denotes the two propagating modes,

$$\left(\frac{c}{\omega}\right)^2 k_\pm^2 = N_\pm^2 \equiv \left(\frac{\det\hat{\varepsilon}_e}{\varepsilon_{yy}^{(e)}}\right)\left[\frac{(\eta_{zz}+\eta_{xx})}{2} \pm \sqrt{\frac{(\eta_{zz}-\eta_{xx})^2}{4} + \eta_{zx}\eta_{xz}}\right], \tag{5}$$

where $\hat{\eta} = 1/\hat{\varepsilon}_e$ is the inverse permittivity tensor.

Thus, there are four solutions to Eq. (5): Two of them represent forward-propagating waves with $k_\pm = (\frac{\omega}{c})\sqrt{N_\pm^2}$, while the other two represent backward-propagating waves with $k_\pm = -(\frac{\omega}{c})\sqrt{N_\pm^2}$. Therefore, a plane-polarized wave normally incident at the sample surface evolves into a refracted wave and a reflected wave. Note again that, in general, all components of the permittivity tensor $\hat{\varepsilon}_e$ can be nonzero (see Fig. 2).

When the externally applied magnetic field vanishes, Eq. (5) simplifies to the form [37–41]

$$\left(\frac{c}{\omega}\right)^2 k_\pm^2 = N_\pm^2 \equiv \varepsilon_{zz}^{(e)} = \varepsilon_{xx}^{(e)}. \tag{6}$$

In Fig. 3(a) we plot numerical results for the case $\mathbf{B}_0 = 0$. The behavior of the position-dependent phase $yk_\pm = (\omega_p/\omega)(\omega_p y/c)\sqrt{\varepsilon_{zz}^{(e)}}$ is determined by the permittivity tensor component $\varepsilon_{zz}^{(e)}$, which has a surface plasmon resonance at $\omega = \omega_p/\sqrt{2}$ for an isolated circular cylinder.

When the magnetic field is directed along the z axis, $\mathbf{B}_0 \parallel z \parallel (001)$, which coincides with the principal symmetry axis (001), Eq. (5) simplifies to the form [37–41]

$$\left(\frac{c}{\omega}\right)^2 k_-^2 = N_-^2 \equiv \varepsilon_{zz}^{(e)}, \tag{7}$$

$$\left(\frac{c}{\omega}\right)^2 k_+^2 = N_+^2 \equiv \varepsilon_{xx}^{(e)} - \frac{\varepsilon_{xy}^{(e)}\varepsilon_{yx}^{(e)}}{\varepsilon_{yy}^{(e)}}. \tag{8}$$

Results for this case are shown in Fig. 3(b). The term N_-^2 is again determined by $\varepsilon_{zz}^{(e)}$. This tensor component has a surface plasmon resonance at the frequency $\omega_{\rm res} \simeq \omega_p/\sqrt{2}$, which is close to the resonance frequency of an isolated cylinder for the case $\mathbf{B}_0 = 0$.

When the magnetic field is perpendicular to the film, $\mathbf{B}_0 \parallel y$, Eq. (5) simplifies to the form [37–41]

$$\left(\frac{c}{\omega}\right)^2 k_\pm^2 = N_\pm^2 = \frac{1}{2}\left(\varepsilon_{xx}^{(e)} + \varepsilon_{zz}^{(e)}\right) \pm \frac{1}{2}\sqrt{\left(\varepsilon_{zz}^{(e)} - \varepsilon_{xx}^{(e)}\right)^2 + 4\varepsilon_{xz}^{(e)}\varepsilon_{zx}^{(e)}}. \tag{9}$$

This equation describes the Faraday effect.

When $\mathbf{B}_0$ is directed not along the principal symmetry axes, the behavior of the wave vectors $k_\pm$ is more complicated

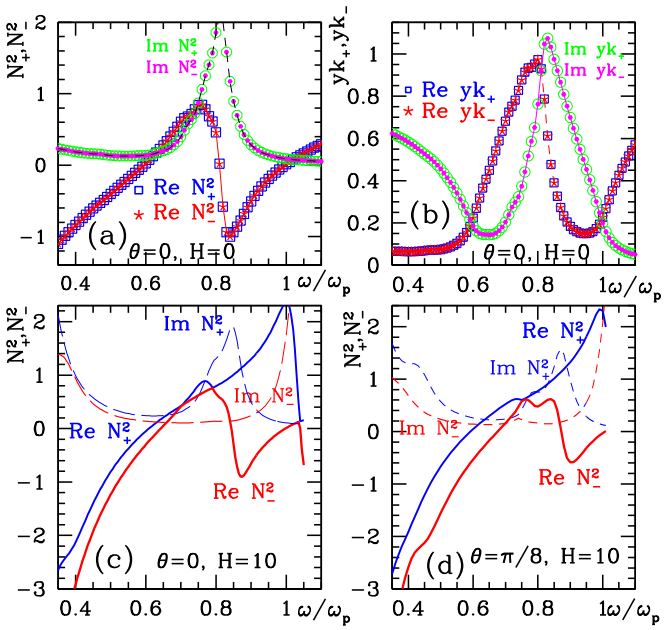

FIG. 3. (Color online) Real and imaginary parts of the squared complex refractive index $N_{\pm}^2$ [see Eq. (5)] (a), (c), (d) and dimensionless wave vector $yk_{\pm} = \frac{\omega}{\omega_p}(\frac{\omega_p y}{c})\sqrt{N_{\pm}^2}$ (b) [where y is the wave propagation distance; see text just before Eq. (19)] vs ω/ω_p. Values of N_+^2 (the real part is shown by blue squares while the imaginary part is shown by green circles) and N_-^2 (the real part is shown by red asterisks while the imaginary part is shown by magenta points) in panel (a), as well as values of yk_+ and yk_- in panel (b), coincide for $H = 0$ and $\theta = 0$. At $H \neq 0$ these values (Re N_-^2 shown by red thick solid line, Im N_-^2 shown by red thin dashed line; Re N_+^2 shown by blue thick solid line, Im N_+^2 shown by blue dashed line) do not coincide anymore; see panel (c) obtained for $H = 10$, $\theta = 0$ and panel (d) obtained for $H = 10$, $\theta = \pi/8$. $\omega_p\tau = 20$ and $\omega_p y/c = 1$. The radii of circular cylinder holes in all the results shown here and below are $R = 0.3a$, where a is the lattice constant.

[see Figs. 3(c) and 3(d)]. The polarizations of the normal modes are then usually not circular but elliptical, as shown in Sec. III.

III. ELECTRIC FIELD OF THE LIGHT BEAM INSIDE THE METAMATERIALS

By substituting each solution of Eq. (5) into Eqs. (2)–(4) we find expressions for the electric field components $E_{z\pm}$ and $E_{y\pm}$ for given E_x. We thus get

$$E_{z\pm} = \frac{N_{\pm}^2 - \varepsilon_{xx}^{(e)} + \frac{\varepsilon_{xy}^{(e)}\varepsilon_{yx}^{(e)}}{\varepsilon_{yy}^{(e)}}}{\varepsilon_{xz}^{(e)} - \frac{\varepsilon_{xy}^{(e)}\varepsilon_{yz}^{(e)}}{\varepsilon_{yy}^{(e)}}} E_{x\pm} = -\frac{\Delta \pm \sqrt{\Delta^2 + 4\chi\eta^2}}{2\chi\eta} E_{x\pm}, \tag{10}$$

$$E_{y\pm} = -\frac{\varepsilon_{yx}^{(e)}}{\varepsilon_{yy}^{(e)}} E_{x\pm} - \frac{\varepsilon_{yz}^{(e)}}{\varepsilon_{yy}^{(e)}} E_{z\pm} = -\left[\left(\frac{\varepsilon_{yx}^{(e)}}{\varepsilon_{yy}^{(e)}}\right) - \left(\frac{\varepsilon_{yz}^{(e)}}{\varepsilon_{yy}^{(e)}}\right)\frac{\Delta \pm \sqrt{\Delta^2 + 4\chi\eta^2}}{2\chi\eta}\right] E_{x\pm}, \tag{11}$$

where we have introduced the definitions $\Delta \equiv \eta_{xx} - \eta_{zz}$, $\eta \equiv \eta_{xz} = \chi\eta_{zx}$ and where the parameter χ is equal to $+1$ or -1 depending on whether $\eta_{xz} = \eta_{zx}$ (in Voigt configuration) or $\eta_{xz} = -\eta_{zx}$ (in Faraday configuration). Note that in those cases $\chi^2 = 1$. That is, for the forward-propagating waves we can write

$$\begin{pmatrix} E_{x\pm} \\ E_{y\pm} \\ E_{z\pm} \end{pmatrix} = A_{\pm} \begin{pmatrix} 1 \\ \beta_{\pm} \\ \alpha_{\pm} \end{pmatrix} \exp[i(\omega t - k_{\pm} y)], \tag{12}$$

where $A_{\pm}$ are arbitrary amplitudes and

$$\beta_{\pm} \equiv -\left[\left(\frac{\varepsilon_{yx}^{(e)}}{\varepsilon_{yy}^{(e)}}\right) - \left(\frac{\varepsilon_{yz}^{(e)}}{\varepsilon_{yy}^{(e)}}\right)\frac{\Delta \pm \sqrt{\Delta^2 + 4\chi\eta^2}}{2\chi\eta}\right], \tag{13}$$

$$\alpha_{\pm} \equiv -\frac{\Delta \pm \sqrt{\Delta^2 + 4\chi\eta^2}}{2\chi\eta}. \tag{14}$$

Equation (12) represents two elliptically polarized (in x,z-plane) waves propagating along y-axis:

$$\begin{pmatrix} E_{x-} \\ E_{z-} \end{pmatrix} = A_{-} \begin{pmatrix} 1 \\ \alpha_{-} \end{pmatrix} \exp[i(\omega t - k_{-} y)], \tag{15}$$

$$\begin{pmatrix} E_{x+} \\ E_{z+} \end{pmatrix} = A_{+} \begin{pmatrix} 1 \\ \alpha_{+} \end{pmatrix} \exp[i(\omega t - k_{+} y)]. \tag{16}$$

The actual normal components of the propagating electric field can now be written for $t = 0$ in terms of the normal modes of Eqs. (15) and (16) as

$$E_x(y)|_{t=0} = A_- e^{-ik_- y} + A_+ e^{-ik_+ y}, \tag{17}$$

$$E_z(y)|_{t=0} = \alpha_- A_- e^{-ik_- y} + \alpha_+ A_+ e^{-ik_+ y}. \tag{18}$$

Therefore, for $y = 0$ and $t = 0$ we can write $E_x(0) = A_- + A_+$ and $E_z(0) = \alpha_- A_- + \alpha_+ A_+$. From this we get $A_+ = [-\alpha_- E_x(0) + E_z(0)]/(\alpha_+ - \alpha_-)$ and $A_- = [\alpha_+ E_x(0) - E_z(0)]/(\alpha_+ - \alpha_-)$. Using the latter expressions, we get a result for the propagating electric field components E_x, E_z at arbitrary distance y from the surface,

$$\begin{pmatrix} E_x(y) \\ E_z(y) \end{pmatrix} = \begin{pmatrix} \cos\frac{\phi}{2} + i\frac{\alpha_+ + \alpha_-}{\alpha_+ - \alpha_-}\sin\frac{\phi}{2} & \frac{-2i}{\alpha_+ - \alpha_-}\sin\frac{\phi}{2} \\ \frac{-2i\chi}{\alpha_+ - \alpha_-}\sin\frac{\phi}{2} & \cos\frac{\phi}{2} - i\frac{\alpha_+ + \alpha_-}{\alpha_+ - \alpha_-}\sin\frac{\phi}{2} \end{pmatrix} \times \begin{pmatrix} E_x(0) \\ E_z(0) \end{pmatrix} e^{i[\omega t - (k_+ + k_-)\frac{y}{2}]}, \tag{19}$$

where $\phi \equiv y(k_+ - k_-)$ and where the matrix we have used is known as the "Jones matrix" and where $\alpha_+\alpha_- = -\chi$ [see Eq. (14)]. The phase difference ϕ is given by

$$\phi = \frac{\omega}{\omega_p}\left(\frac{\omega_p y}{c}\right)(N_+ - N_-). \tag{20}$$

The real part of ϕ is responsible for the magnetic birefringence. We recall that $k_{\pm}$ are the wave-number eigenvalues of Eqs. (3) and (4), which correspond to the appropriate choice of sign before the square root in Eq. (5) and $N_{\pm}$ is the complex refractive index ($n'_{\pm} = \mathrm{Re}N_{\pm}$). Equations (5)–(20) are valid for any direction of the applied magnetic field and this includes both Faraday and Voigt configurations.

If ϕ is real, then expressions for the rotation angle β (the angle of the major axis of the ellipse with respect to the x axis of the ellipse of the incident light polarization) and for the ellipticity κ [the ratio of the minor to major axes of the polarization ellipse (see Appendix B)] can be found in simple closed form [31]. Below we consider a more general (and more complicated) case where the wave numbers $k_\pm$ and the phase difference ϕ are complex valued and the optical geometry is not restricted to the Faraday configuration.

IV. POLARIZATION ROTATION AND ELLIPTICITY IN THE GENERAL CASE

A. General case

Let a plane wave polarized along the x direction with unit amplitude ($E_{x0}=1$, $E_{z0}=0$) be incident upon the composite medium. It follows from Eq. (19) that, at a distance y from the sample surface, we have the following x and z components of the electric field,

$$E_x(y)=\left[\cos\frac{\phi}{2}-i\frac{\Delta}{\sqrt{\Delta^2+4\chi\eta^2}}\sin\frac{\phi}{2}\right]e^{i[\omega t-(k_++k_-)\frac{y}{2}]}E_{x0}$$
$$=\mathcal{E}_x e^{i\delta_x}e^{i[\omega t-(k_++k_-)\frac{y}{2}]}E_{x0}, \tag{21}$$

$$E_z(y)=\frac{2i\eta}{\sqrt{\Delta^2+4\chi\eta^2}}\sin\frac{\phi}{2}e^{i[\omega t-(k_++k_-)\frac{y}{2}]}E_{x0}$$
$$=\mathcal{E}_z e^{i\delta_z}e^{i[\omega t-(k_++k_-)\frac{y}{2}]}E_{x0}, \tag{22}$$

where the values of the parameters $\mathcal{E}_x$, δ_x, $\mathcal{E}_z$, δ_z can be found either numerically [$\mathcal{E}_x=\sqrt{A^2+B^2}$, $\delta_x=\arctan(B/A)$, where $A+iB\equiv\cos\frac{\phi}{2}-i(\Delta\sin\frac{\phi}{2})/\sqrt{\Delta^2+4\chi\eta^2}$, and similarly, $\mathcal{E}_z=\sqrt{\tilde{A}^2+\tilde{B}^2}$, $\delta_z=\arctan(\tilde{B}/\tilde{A})$, where $\tilde{A}+i\tilde{B}\equiv 2i(\eta\sin\frac{\phi}{2})/\sqrt{\Delta^2+4\chi\eta^2}$], or algebraically. Note also that η, Δ, ϕ, etc., are complex valued ($\eta=\eta'+i\eta''$, $\Delta=\Delta'+i\Delta''$, $\phi=\phi'+i\phi''$, etc.) and therefore $\sin(\frac{\phi'}{2}+i\frac{\phi''}{2})=\sin\frac{\phi'}{2}\cosh\frac{\phi''}{2}+i\cos\frac{\phi'}{2}\sinh\frac{\phi''}{2}$, $\cos(\frac{\phi'}{2}+i\frac{\phi''}{2})=\cos\frac{\phi'}{2}\cosh\frac{\phi''}{2}-i\sin\frac{\phi'}{2}\sinh\frac{\phi''}{2}$.

As soon as the electric field of the EM wave is written in the form $\mathcal{E}_x e^{i\delta_x}$, $\mathcal{E}_z e^{i\delta_z}$ [see Eqs. (21) and (22)], the rotation angle β of the polarized electric vector $\mathbf{E}_0$ and its ellipticity κ can be expressed through the ratio $|E_x|/|E_z|$ (see Refs. [31,37,38]) or through the related Stokes parameters (see Ref. [42]),

$$\tan 2\beta=\frac{2\mathcal{E}_x\mathcal{E}_z}{\mathcal{E}_x^2-\mathcal{E}_z^2}\cos(\delta_x-\delta_z), \tag{23}$$

$$\sin 2\kappa=-\frac{2\mathcal{E}_x\mathcal{E}_z}{\mathcal{E}_x^2+\mathcal{E}_z^2}\sin(\delta_x-\delta_z), \tag{24}$$

where, as was mentioned above, the parameters $\mathcal{E}_x$, $\mathcal{E}_z$, δ_x, and δ_z [see Eqs. (21) and (22)] can be found either numerically or algebraically (see Appendixes A and B).

B. Faraday configuration

In Faraday configuration the magnetic field $\mathbf{B}_0$ is directed along the y axis perpendicular to the x,z-film plane (see Fig. 1). In this case, the Hall (and only nonzero off-diagonal) components are $\varepsilon_{xz}^{(e)}=-\varepsilon_{zx}^{(e)}$, i.e., $\chi=-1$. Since we consider a symmetric (in x and z directions) microstructure, Eqs. (21) and (22) simplify drastically. In this case, $\eta_{xx}=\eta_{zz}$ and therefore $\Delta=0$. Then the only nonzero components of the tensor $\hat{\eta}$ are the following:

$$\eta_{xx}=\eta_{yy}=\frac{\varepsilon_{xx}^{(e)}}{\varepsilon_{xx}^{(e)2}+\varepsilon_{xz}^{(e)2}}, \tag{25}$$

$$\eta_{xz}=-\eta_{zx}=\frac{\varepsilon_{zx}^{(e)}}{\varepsilon_{xx}^{(e)2}+\varepsilon_{xz}^{(e)2}}, \tag{26}$$

$$\eta_{zz}=\frac{\varepsilon_{zz}^{(e)}}{\varepsilon_{xx}^{(e)2}+\varepsilon_{xz}^{(e)2}}. \tag{27}$$

Equations (21) and (22) then take the form

$$E_x(y)=\cos\frac{\phi}{2}e^{i[\omega t-(k_++k_-)\frac{y}{2}]}E_{x0}, \tag{28}$$

$$E_z(y)=\sin\frac{\phi}{2}e^{i[\omega t-(k_++k_-)\frac{y}{2}]}E_{x0}, \tag{29}$$

where $\phi=y(k_+-k_-)$ and $k_\pm=(\omega/c)\sqrt{\varepsilon_{xx}^{(e)}\pm i\varepsilon_{xz}^{(e)}}$ [see Eqs. (9) and (20)]. If $\varepsilon_{xz}^{(e)}\ll 1$, then $\phi\simeq(\omega y/c)\,i\varepsilon_{xz}^{(e)}/\sqrt{\varepsilon_{xx}^{(e)}}$.

V. VOLUME-AVERAGED EFFECTIVE PERMITTIVITY TENSOR AND CALCULATIONAL SCHEME

In order to observe and study the expected anisotropy of the MO response of ordered metal-dielectric composites in the quasistatic regime we applied a calculational approach similar to what had been used earlier for the magneto-transport response [1,43–49]. Following Refs. [3,4,32–34], we treated the perforated metal film as insulating inclusions embedded in a metal host. Following Ref. [46] we chose a scheme where the composite medium occupies the entire volume between the infinitely conducting plates of a large parallel plate capacitor. The electric potential field ϕ of the considered system is the solution of the partial differential equation $\nabla\cdot\mathbf{D}=0$, namely,

$$\nabla\cdot\hat{\varepsilon}_2\cdot\nabla\phi^{(\alpha)}=\nabla\cdot\theta_1\delta\hat{\varepsilon}\cdot\nabla\phi^{(\alpha)}, \tag{30}$$

with the boundary condition $\phi^{(\alpha)}=r_\alpha$. Here $\mathbf{D}$ is the electric displacement field, $\delta\hat{\varepsilon}\equiv\hat{\varepsilon}_2-\hat{\varepsilon}_1$, where $\hat{\varepsilon}_1$ and $\hat{\varepsilon}_2$ are the electrical permittivity tensors of the (dielectric) holes and the *metal* film (host), respectively, and $\theta_1(\mathbf{r})$ is the characteristic function describing the location and shape of the holes ($\theta_1=0$ inside the holes and $\theta_1=1$ outside of them) [4].

The left-hand side of Eq. (30) is simple enough (i.e., a second-order elliptic differential operator with constant coefficients) that it is useful to define its Green's function $G(\mathbf{r},\mathbf{r}'|\hat{\varepsilon}_2)$:

$$\nabla\cdot\hat{\varepsilon}_2\cdot\nabla G=-\delta^3(\mathbf{r}-\mathbf{r}') \quad \text{for} \quad \mathbf{r}\in V, \tag{31}$$

$$G=0 \quad \text{for} \quad \mathbf{r}\in\partial V. \tag{32}$$

Note that G depends only on the symmetric part of the tensor $\hat{\varepsilon}_2$. Using G, we can transform the boundary value problem of Eq. (30) to an integro-differential equation

for $\phi(\mathbf{r})$,

$$\phi = -\mathbf{E}_0 \cdot \mathbf{r} - \int dV' G(\mathbf{r},\mathbf{r}'|\hat{\varepsilon}_2)\nabla' \cdot (\theta_1' \delta\hat{\varepsilon} \cdot \nabla'\phi') = -\mathbf{E}_0 \cdot \mathbf{r} + \int dV' \theta_1' (\nabla' G \cdot \delta\hat{\varepsilon} \cdot \nabla'\phi') \quad (33)$$

$$= r_\alpha + \hat{\Gamma}\phi^{(\alpha)}, \quad (34)$$

where we used integration by parts to get the second line and where the linear integro-differential operator $\hat{\Gamma}$ is defined by

$$\hat{\Gamma}\phi \equiv \int dV' \theta_1(\mathbf{r}')\nabla' G(\mathbf{r},\mathbf{r}'|\hat{\varepsilon}_2) \cdot \delta\hat{\varepsilon} \cdot \nabla'\phi(\mathbf{r}'). \quad (35)$$

The electric field, $\mathbf{E} = -\nabla\phi$, therefore, has the form

$$\mathbf{E}(\mathbf{r}) = -\nabla\phi = \mathbf{E}_0 + \int dV' \theta_1' \nabla\nabla' G \cdot \delta\hat{\varepsilon} \cdot \mathbf{E}'. \quad (36)$$

Here we used the abbreviated notation ϕ' for $\phi(\mathbf{r}')$, etc. When V is infinite, $G(\mathbf{r},\mathbf{r}'|\hat{\varepsilon})$ depends only on the separation vector $\mathbf{r} - \mathbf{r}'$. The Fourier transform of G then has the simple form

$$\int dV e^{-\mathbf{k}\cdot(\mathbf{r}-\mathbf{r}')} G(\mathbf{r},\mathbf{r}'|\hat{\varepsilon}) = \frac{1}{(\mathbf{k} \cdot \hat{\varepsilon} \cdot \mathbf{k})}. \quad (37)$$

Although G, and hence also $\hat{\Gamma}$, depend on the orientation of the capacitor plates, this dependence is only important if at least one of $\mathbf{r}$, $\mathbf{r}'$ is near the plates. For most purposes G can be approximated by the Green's function that vanishes at infinity, and in that case the only dependence of (34) on the boundary conditions comes from the term r_α, which ensures that $\phi^{(\alpha)}$ satisfies them. The microstructure enters into $\hat{\Gamma}$ through the characteristic function $\theta_1(\mathbf{r})$. Due to the symmetric dot products of $\hat{\varepsilon}_2$ and the two ∇ operators in (31), the antisymmetric part of $\hat{\varepsilon}_2$ does not participate in that equation. Therefore, $G(\mathbf{r},\mathbf{r}'|\hat{\varepsilon}_2)$ actually only depends on the symmetric part $\hat{\varepsilon}_{2s}$ of $\hat{\varepsilon}_2$. The Green's function that vanishes at infinity depends on $\mathbf{r}$, $\mathbf{r}'$ only through their difference $\mathbf{r} - \mathbf{r}'$. In the case where $\hat{\varepsilon}_{2s}$ is a diagonal tensor, this Green's function has a relatively simple closed form, namely [1,46,48],

$$G(\mathbf{r},\mathbf{r}'|\hat{\varepsilon}) = \frac{1}{4\pi(\varepsilon_{xx}\varepsilon_{yy}\varepsilon_{zz})^{1/2}} \times \left[\frac{(x-x')^2}{\varepsilon_{xx}} + \frac{(y-y')^2}{\varepsilon_{yy}} + \frac{(z-z')^2}{\varepsilon_{zz}}\right]^{-1/2}. \quad (38)$$

The distorted part of $\phi^{(\alpha)}(\mathbf{r})$ is defined by

$$\psi^{(\alpha)}(\mathbf{r}) \equiv \phi^{(\alpha)}(\mathbf{r}) - r_\alpha, \quad (39)$$

and satisfies an integral equation which immediately follows from (34)

$$\psi^{(\alpha)} = \hat{\Gamma} r_\alpha + \hat{\Gamma}\psi^{(\alpha)}. \quad (40)$$

This equation can be solved symbolically by using the resolvent operator $1/(1 - \hat{\Gamma})$

$$\psi^{(\alpha)}(\mathbf{r}) = \frac{\hat{\Gamma}}{1 - \hat{\Gamma}} r_\alpha. \quad (41)$$

While it is usually impossible to calculate the resolvent operator in closed form, it is sometimes useful to expand it as a series in powers of $\hat{\Gamma}$ or $\delta\hat{\varepsilon}$.

The bulk effective electric permittivity tensor, $\hat{\varepsilon}_e$, is defined as providing the linear relationship between volume averages of the two fields, $\mathbf{E}$, $\mathbf{D}$:

$$\langle \mathbf{D} \rangle \equiv \hat{\varepsilon}_e \cdot \langle \mathbf{E}(\mathbf{r}) \rangle. \quad (42)$$

The final result for $\hat{\varepsilon}_e$ will be independent of the precise way in which the local electric field is created, provided that the composite microstructure, as well as the boundary conditions that determine $\mathbf{E}(\mathbf{r})$, are macroscopically homogeneous. We are therefore free to choose the most convenient boundary conditions when setting up a scheme for calculating $\mathbf{E}(\mathbf{r})$.

Using (42) we can write for $\hat{\varepsilon}_e$

$$\hat{\varepsilon}_e \cdot \langle \nabla\phi^{(\alpha)} \rangle = \hat{\varepsilon}_2 \cdot \langle \nabla\phi^{(\alpha)} \rangle - \delta\hat{\varepsilon} \cdot \langle \theta_1 \nabla\phi^{(\alpha)} \rangle. \quad (43)$$

This expression can be further processed by using (39) and recalling that $\langle \nabla\phi^{(\alpha)} \rangle = \mathbf{e}_\alpha$. In this way we get

$$(\hat{\varepsilon}_2 - \hat{\varepsilon}_e) \cdot \mathbf{e}_\alpha = \delta\hat{\varepsilon} \cdot \langle \theta_1 \nabla r_\alpha \rangle + \delta\hat{\varepsilon} \cdot \langle \theta_1 \nabla\psi^{(\alpha)} \rangle, \quad (44)$$

which reduces to

$$(\hat{\varepsilon}_2 - p_1\delta\hat{\varepsilon} - \hat{\varepsilon}_e)_{\alpha\beta} = \delta\hat{\varepsilon}_{\alpha\gamma} \langle \theta_1 \nabla_\gamma \psi^{(\beta)} \rangle, \quad (45)$$

where $p_1 \equiv \langle \theta_1 \rangle$ is the volume fraction of the $\hat{\varepsilon}_1$ constituent. Here and in the rest of this article we use the convention that a summation over repeated tensor indices is always implied.

When the composite medium has a periodic microstructure, great simplifications ensue due to the fact that $\theta_1(\mathbf{r})$ is now a periodic function. From the fact that, away from the external boundaries, G depends on $\mathbf{r}$, $\mathbf{r}'$ only through their difference $\mathbf{r} - \mathbf{r}'$ [see Eq. (38)], we get that for any periodic or linear function $f(\mathbf{r})$, $\hat{\Gamma} f$ is also periodic except near those boundaries. Hence, $\psi^{(\alpha)}(\mathbf{r})$ is periodic and can be expanded in a Fourier series

$$\psi^{(\alpha)}(\mathbf{r}) = \sum_{\mathbf{g}} \psi_{\mathbf{g}}^{(\alpha)} e^{i\mathbf{g}\cdot\mathbf{r}}, \quad (46)$$

where the sum is over all the vectors $\mathbf{g} = (2\pi/a)(m_x, m_y, m_z)$ of the appropriate reciprocal lattice, m_i are arbitrary integers, and a is the lattice constant. The Fourier expansion coefficient of an arbitrary periodic function $f(\mathbf{r})$ is given by

$$f_{\mathbf{g}} = \frac{1}{V_a} \int_{V_a} dV e^{-i\mathbf{g}\cdot\mathbf{r}} f(\mathbf{r}), \quad (47)$$

where V_a is the volume of one-unit cell.

The Fourier transform of G [see Eq. (38)] which vanishes at infinity has an even simpler form, namely,

$$\int dV e^{-i\mathbf{k}\cdot(\mathbf{r}-\mathbf{r}')} G(\mathbf{r},\mathbf{r}'|\hat{\varepsilon}_{2s}) = \frac{1}{\mathbf{k} \cdot \hat{\varepsilon}_{2s} \cdot \mathbf{k}}, \quad (48)$$

which is valid regardless of the detailed form of $\hat{\varepsilon}_{2s}$. This result is easily obtained by performing a Fourier transformation of (31).

Instead of the Fourier coefficients $f_{\mathbf{g}}$ [see Eq. (47)], it is convenient to introduce the following coefficients:

$$i(\mathbf{g} \cdot \hat{\varepsilon}_2 \cdot \mathbf{g})^{1/2} f_{\mathbf{g}} = i(\mathbf{g} \cdot \hat{\varepsilon}_{2s} \cdot \mathbf{g})^{1/2} f_{\mathbf{g}} \quad \text{for} \quad \mathbf{g} \neq 0. \quad (49)$$

These characterize the function $f(\mathbf{r})$ up to an additive constant.

Some straightforward calculations lead to the following results for the Fourier coefficients of $\hat{\Gamma} r_\alpha$ and $\hat{\Gamma} f$, where $f(\mathbf{r})$ is an arbitrary periodic function,

$$i(\mathbf{g}\cdot\hat{\varepsilon}_{2s}\cdot\mathbf{g})^{1/2}(\hat{\Gamma} r_\alpha)_{\mathbf{g}} = \frac{g_\beta \delta\varepsilon_{\beta\alpha}\theta_{\mathbf{g}}}{(\mathbf{g}\cdot\hat{\varepsilon}_{2s}\cdot\mathbf{g})^{1/2}}, \tag{50}$$

$$i(\mathbf{g}\cdot\hat{\varepsilon}_{2s}\cdot\mathbf{g})^{1/2}(\hat{\Gamma} f)_{\mathbf{g}} = \sum_{\mathbf{g}'\neq 0}\Gamma_{\mathbf{g}\mathbf{g}'} i(\mathbf{g}'\cdot\hat{\varepsilon}_{2s}\cdot\mathbf{g}')^{1/2} f_{\mathbf{g}'}, \tag{51}$$

$$\Gamma_{\mathbf{g}\mathbf{g}'} \equiv \frac{(\mathbf{g}\cdot\delta\hat{\varepsilon}\cdot\mathbf{g}')}{(\mathbf{g}\cdot\hat{\varepsilon}_{2s}\cdot\mathbf{g})^{1/2}(\mathbf{g}'\cdot\hat{\varepsilon}_{2s}\cdot\mathbf{g}')^{1/2}}\theta_{\mathbf{g}-\mathbf{g}'}, \tag{52}$$

where $\theta_{\mathbf{g}}$ is the Fourier coefficient of $\theta_1(\mathbf{r})$. Clearly, the matrix defined in (52) represents the integro-differential operator $\hat{\Gamma}$ in this scheme.

We now translate the integro-differential equation (40) for $\psi^{(\alpha)}(\mathbf{r})$ into an infinite set of linear algebraic equations for the Fourier coefficients $\psi^{(\alpha)}_{\mathbf{g}}$, which are represented by

$$a^{(\alpha)}_{\mathbf{g}} \equiv i(\mathbf{g}\cdot\hat{\varepsilon}_{2s}\cdot\mathbf{g})^{1/2}\psi^{(\alpha)}_{\mathbf{g}} \quad \text{for} \quad \mathbf{g}\neq 0. \tag{53}$$

This is done by Fourier transforming (40) and using (50) and (51) and leads to

$$a^{(\alpha)}_{\mathbf{g}} = r^{(\alpha)}_{\mathbf{g}} + \sum_{\mathbf{g}'\neq 0}\Gamma_{\mathbf{g}\mathbf{g}'} a^{(\alpha)}_{\mathbf{g}'} \quad \text{for} \quad \mathbf{g}\neq 0, \tag{54}$$

$$r^{(\alpha)}_{\mathbf{g}} \equiv \frac{g_\beta \delta\varepsilon_{\beta\alpha}}{(\mathbf{g}\cdot\hat{\varepsilon}_{2s}\cdot\mathbf{g})^{1/2}}\theta_{\mathbf{g}}. \tag{55}$$

Solving a finite subset of the linear equations (54) for the Fourier expansion coefficients $a^{(\alpha)}_{\mathbf{g}}$, one can write for the electrical potential $\phi^{(\alpha)}$

$$\phi^{(\alpha)} = r_\alpha + \psi^{(\alpha)} = r_\alpha + \sum_{\mathbf{g}}\frac{a^{(\alpha)}_{\mathbf{g}}}{i(\mathbf{g}\cdot\hat{\varepsilon}_{2s}\cdot\mathbf{g})^{1/2}}e^{i\mathbf{g}\cdot\mathbf{r}} \tag{56}$$

and for the bulk effective permittivity tensor

$$\begin{aligned}(\hat{\varepsilon}_2 - p_1\delta\hat{\varepsilon} - \hat{\varepsilon}_e)_{\alpha\beta} &= \frac{\delta\varepsilon_{\alpha\gamma}}{V_a}\int_{V_a} dV\theta_1(\mathbf{r})\sum_{\mathbf{g}} i g_\gamma \psi^{(\beta)}_{\mathbf{g}} e^{i\mathbf{g}\cdot\mathbf{r}} \\ &= \delta\varepsilon_{\alpha\gamma}\sum_{\mathbf{g}} i g_\gamma \psi^{(\beta)}_{\mathbf{g}}\theta_{-\mathbf{g}} \\ &= \sum_{\mathbf{g}\neq 0}\frac{\delta\varepsilon_{\alpha\beta}g_\beta}{(\mathbf{g}\cdot\hat{\varepsilon}_{2s}\cdot\mathbf{g})^{1/2}}\theta_{-\mathbf{g}}a^{(\beta)}_{\mathbf{g}}.\end{aligned} \tag{57}$$

Note that the coefficient multiplying $a^{(\beta)}_{\mathbf{g}}$ in the last sum looks similar to $r^{(\alpha)*}_{\mathbf{g}}$, but actually differs from it, because $\delta\varepsilon_{\alpha\beta} \neq \delta\varepsilon^*_{\beta\alpha}$.

In light of the above discussion, a finite subset of Eqs. (54) and (55) was solved numerically and used to compute $\hat{\varepsilon}_e$ [using Eq. (57)] [1,46]. That was then used to implement a computational analysis of the Faraday and Voigt effects in various metal-dielectric composites with a periodic microstructure.

Note also that in order to simplify the numerical procedure, we calculate the permittivity tensor $\hat{\varepsilon}_e$ for the system of a three-dimensional composite with a two-dimensional columnar microstructure: The finite cylinders become infinitely long cylinders with axes parallel to y, while the finite film thickness ℓ is taken into account by using the proper analytical expressions for the macroscopic MO response. This drastically simplifies the calculations but does not qualitatively change the final result as long as $\ell H > a$ [50].

The metal permittivity tensor $\hat{\varepsilon}_1 = \hat{\varepsilon}_M$ has the form [3–6,11,43,51,52]

$$\begin{aligned}\hat{\varepsilon}_M &= \varepsilon_0\cdot\hat{I} + i\frac{4\pi}{\omega}\hat{\sigma} = \varepsilon_0\cdot\hat{I} \\ &+ \frac{i\omega_p^2\tau}{\omega}\begin{pmatrix}\frac{1-i\omega\tau}{(1-i\omega\tau)^2+H^2} & \frac{-H}{(1-i\omega\tau)^2+H^2} & 0\\ \frac{H}{(1-i\omega\tau)^2+H^2} & \frac{1-i\omega\tau}{(1-i\omega\tau)^2+H^2} & 0\\ 0 & 0 & \frac{1}{1-i\omega\tau}\end{pmatrix},\end{aligned} \tag{58}$$

where the conductivity tensor $\hat{\sigma}$ is taken in the Drude approximation (with $\mathbf{B}_0 \parallel z$), ε_0 is the scalar dielectric constant of the background ionic lattice, which we take to be 1 in this article, and $\hat{I}$ is the unit tensor. The applied magnetic field $\mathbf{B}_0$ enters only through the Hall-to-Ohmic resistivity ratio $H \equiv \rho_H/\rho = \sigma_{yx}/\sigma_{xx} = \mu_H|\mathbf{B}_0| = \omega_c\tau$, where $\omega_c = e|\mathbf{B}_0|/mc$ is the cyclotron frequency, τ is the conductivity relaxation time, $\omega_p = \left(4\pi e^2 N_0/\varepsilon_0 m\right)^{1/2}$ is the bulk plasma frequency, N_0 is the charge carrier concentration, m is the effective mass of the charge carriers, and μ_H is the Hall mobility [3,4,11,43].

VI. NUMERICAL RESULTS

A. Voigt configuration

When both $\mathbf{B}_0$ and $\mathbf{E}$ are rotated in the film plane [see Fig. 1(b)], all components of the permittivity tensor $\hat{\varepsilon}_e$ can be nonzero and their angular profiles are anisotropic [3,4] (this is similar to the magneto-induced angular anisotropy of magnetoresistance [1,5,6,43–46,49–52]). The angular profiles of the diagonal components $\varepsilon^{(e)}_{xx}$, $\varepsilon^{(e)}_{yy}$, $\varepsilon^{(e)}_{zz}$ and the off-diagonal components $\varepsilon^{(e)}_{xy}$, $\varepsilon^{(e)}_{xz}$, $\varepsilon^{(e)}_{yx}$, $\varepsilon^{(e)}_{yz}$, $\varepsilon^{(e)}_{zx}$, and $\varepsilon^{(e)}_{zy}$ in nonrotating and rotating coordinate systems are shown in Fig. 2. Here and everywhere below we perform numerical calculations for the metamaterial sample, made of a simple-square array (with lattice constant a) of perpendicular circular cylinder holes (of radius $R = 0.3a$) in a metal film.

In Fig. 3 [see panels (a), (c), and (d)] we show the real and imaginary parts of the squared refractive indices N^2_+ and N^2_-, as well as the real and imaginary parts of of the dimensionless wave vectors $yk_\pm$ vs ω/ω_p, where y is the distance traversed by the propagating wave in the composite. Here and everywhere below it is assumed that $\omega y/c \sim 1$, which is a realistic situation (see Ref. [16]). When $H = 0$, the permittivity tensor in the film plane is isotropic ($\varepsilon^{(e)}_{xx} = \varepsilon^{(e)}_{zz}$), and its off-diagonal component $\varepsilon^{(e)}_{xz}$ vanishes. From Eq. (5) it then follows that $N^2_+ = N^2_-$ and $k_+ = k_-$.

By contrast, when $H \neq 0$ the permittivity tensor $\hat{\varepsilon}_e$ and its inverse $\hat{\eta}$ are not isotropic ($\varepsilon^{(e)}_{xx} \neq \varepsilon^{(e)}_{zz}$, $\eta_{xx} \neq \eta_{zz}$), while the value of $\varepsilon^{(e)}_{xz}$ depends on the direction of $\mathbf{B}_0$ with respect to the microstructure axes. When $\theta = 0$ the non-Hall off-diagonal components $\varepsilon^{(e)}_{xz}$,$\varepsilon^{(e)}_{yz}$ vanish even for $H \neq 0$. However, at other values of θ, for instance at $\theta = \pi/8$, these off-diagonal components are nonzero and the wave vector k_+ differs significantly from k_- in most frequency ranges [see Fig. 3(d)]. When $k_+ \neq k_-$ it means that the phase shift $\phi \neq 0$ [see Eq. (20)] and we should expect to observe birefringence, rotation of the polarization, and ellipticity.

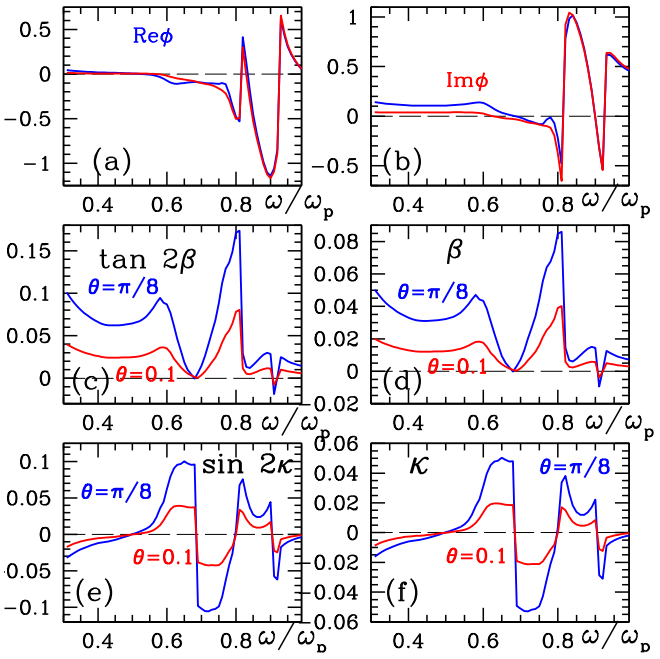

FIG. 4. (Color online) (a), (b) Real and imaginary parts of the phase shift ϕ [see Eq. (20)] vs ω/ω_p, respectively. (c), (d) $\tan 2\beta$ and rotation angle β (in radians) vs. ω/ω_p, respectively. (e), (f) $\sin 2\kappa$ and ellipticity κ [see Eq. (24)] vs ω/ω_p, respectively. The blue and red lines in panels (a)–(f) show the values obtained for $\theta = \pi/8$ and $\theta = 0.1$, respectively. $H = 5$, $\omega_p\tau = 20$, $\omega_p y/c = 1$, and $R = 0.3a$.

In Fig. 4 we show the real and imaginary parts of the phase shift ϕ [see Eq. (20) and Figs. 3(a) and 3(b)] vs ω/ω_p for $H = 10$. As soon as we know the phase shift ϕ, we can

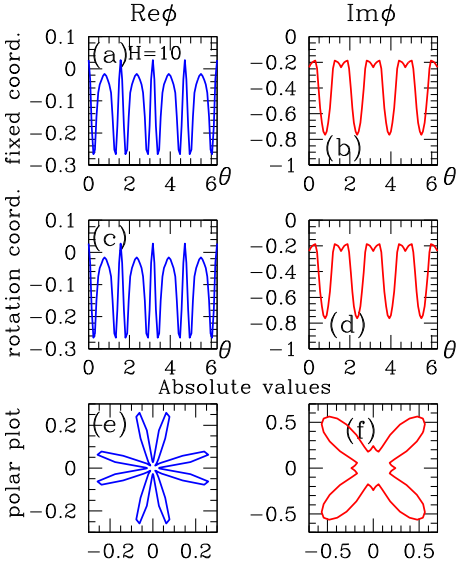

FIG. 5. (Color online) Real and imaginary parts of the phase shift ϕ [see Eq. (20)]. $H = 10$. (a), (b) Cartesian plots in fixed coordinates. (c), (d) Cartesian plots in rotating coordinates. (e), (f) Polar plots of the above quantities. In all the calculations the following parameter values were used: $\omega_p y/c = 1$, $\omega_p\tau = 20$, $\omega = 0.8\omega_p$, $R = 0.3a$.

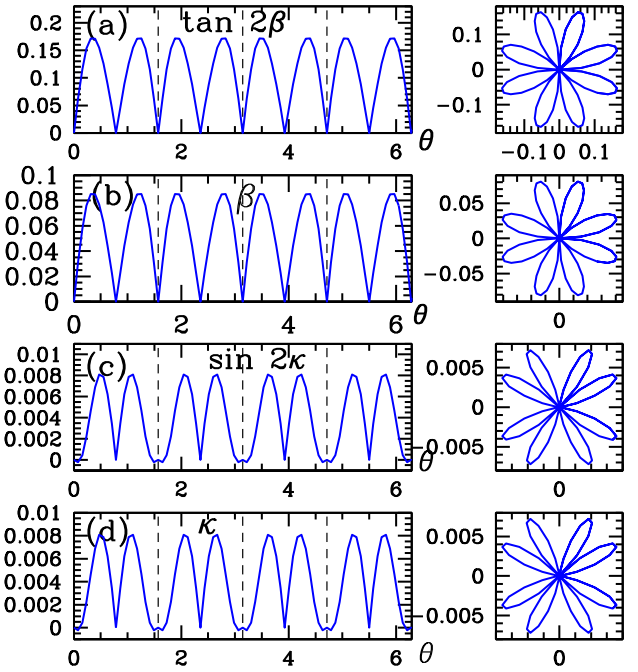

FIG. 6. (Color online) Rotation angle (in the Voigt configuration) β and ellipticity κ vs the angle of rotation θ of the applied magnetic field $\mathbf{B}_0$ (with respect to the main axes of the periodic microstructure) in the rotating coordinate system. In the right column are shown the absolute values of the same quantities as polar plots. (a) $\sin 2\beta$ vs θ; (b) β vs θ; (c) $\sin 2\kappa$ vs θ; (d) Ellipticity κ vs θ. $H = 5$. In all the calculations the following parameter values were used: $\omega_p y/c = 1$, $\omega_p\tau = 20$, $\omega = 0.8\omega_p$, $R = 0.3a$.

calculate $\tan 2\beta$ and the polarization rotation angle β as well as $\sin 2\kappa$ and ellipticity κ using Eq. (24) with $\chi = 1$ (in the Voigt configuration).

In Fig. 5 we show the angular profile of the real and imaginary parts of the phase shift ϕ [see Eq. (20)] in fixed and rotating coordinates for $H = 10$. Note that Figs. 5(c) and 5(d) look the same as Figs. 5(a) and 5(b), despite the fact that they involve different configurations. This is due to the fact that Eq. (5) is invariant under the coordinate rotation (with the rotation axis lying along the light propagation direction): $k_\pm(\hat{R}^{-1}\cdot\hat{\eta}\cdot\hat{R}) = k_\pm(\hat{\eta})$, where $\hat{R} = \{\{\cos\theta, 0, -\sin\theta\}, \{0,1,0\}, \{\sin\theta, 0, \cos\theta\}\}$ is the rotation matrix. Polar plots of the above quantities are shown in Figs. 5(e) and 5(f).

The angular profiles of $\tan\beta$ and the polarization rotation angle β as well as $\sin 2\kappa$ and the ellipticity κ are shown in the left column of Fig. 6 for $\omega = 0.8\omega_p$. As in the previous cases, a strong angular magneto-induced anisotropy of β and κ is observed. Their polar plots are shown in the right column of this figure. These angular profiles and their dependencies on the holes sizes [as well as angular profiles of permittivity tensor components, see Figs. 2(g)–2(i), top and bottom] are qualitatively similar to angular dependencies of the magnetoresistance tensor $\hat{\rho}_e(H) = \hat{\sigma}_e^{-1}(H)$ [1,2,5,6,44,45,50,51]. However, since the permittivity tensor is complex, its quantitative description needs further studies.

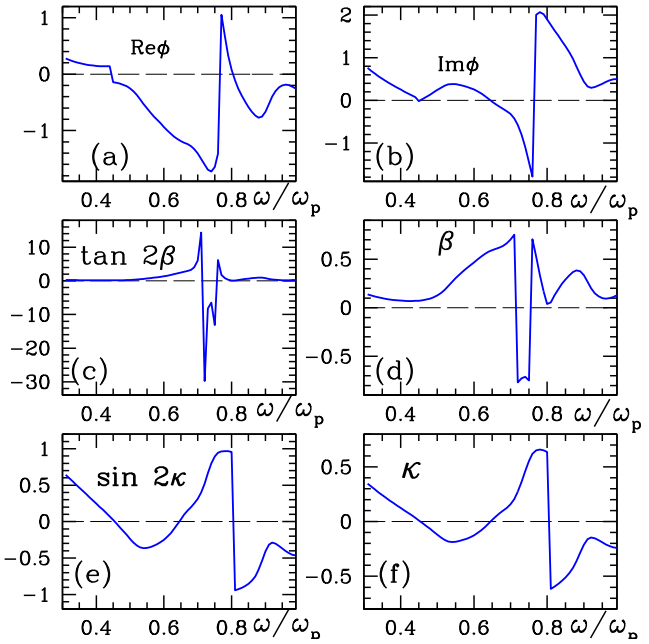

FIG. 7. (Color online) Similar to Fig. 4, but for the Faraday configuration when magnetic field $\mathbf{B}_0$ is perpendicular to the film plane and $\chi = -1$ in Eqs. (10), (11), (21), (22), and (A1)–(A6). All components of the effective permittivity tensor $\hat{\varepsilon}_e$ are calculated along the fixed (not rotating) coordinates, i.e., $\theta = 0$. $H = 5$, $\omega_p\tau = 20$, $\omega_p y/c = 1$, $R = 0.3a$.

B. Faraday configuration

For comparison, we show in Fig. 7 the dependencies similar to Fig. 4, but for the Faraday configuration, when the magnetic field $\mathbf{B}_0$ is perpendicular to the film plane and $\chi = -1$. The effect of rotation of the polarization plane β and the ellipticity κ are much stronger in this case, but there is no magneto-induced angular anisotropy in this case.

VII. SUMMARY AND DISCUSSION

In summary, we have studied analytically and numerically the rotation and ellipticity of polarization of the light propagating through a metamaterial film with periodic microstructure for arbitrary direction of the applied static magnetic field, including both Voigt (when the static magnetic field is in the film plane) and Faraday (when that field is perpendicular to the film) configurations. In the Voigt configuration we found strong dependencies of the above-mentioned effects on the direction of the applied field. The angular anisotropy of other MO effects (including Kerr effect) can be considered similarly. We hope that the results presented here will stimulate experimental studies aimed at verification of our predictions and continued exploration of the MO properties of such systems. This could also form the basis for a new type of MO switch and other MO devices. As a material that may be suitable for the metallic constituent, bismuth can be considered, wherein the low free-charge density ($\sim 3 \times 10^{17}$ cm^{-3}) can make the carrier cyclotron frequency ω_c equal to or greater than the plasma frequency ω_p [6,53–55].

Another possibility is to use a highly doped semiconductor such as GaAs or InAs [3–5]: In that case, it is possible to obtain large values of the Hall mobility μ_H and, therefore, also large values of the dimensionless magnetic field $H = \mu_H|\mathbf{B}_0|$, while using lower values of $\mathbf{B}_0$. The value of $\omega_p\tau$ in this case can be of the same order of magnitude as that of conventional metals in our calculations, where we assumed $\omega_p\tau = 20$. Thus, such magnetic-field-dependent extraordinary optical transmission in the infrared range of frequencies can be sought in heavily doped semiconductor films with an array of holes with a submicrometer periodicity. Detailed estimations of the above-mentioned parameters, which are typical of GaAs and InAs, can be found in Refs. [3–5]. Also to be found there is a discussion of how small the size scale of the microstructure should be in order for the quasistatic limit to be applicable.

In transition-metal films made of Ag or Au, wherein surface plasmons are easily observed in visible light, stronger magnetic fields would be needed in order to observe the behavior described here. This is due to the lower values of the electronic Hall mobility in those metals. A possible way to overcome this handicap would be to use layered ferromagnet-Ag or -Au sandwiches.

It has recently been shown that in a metal-dielectric metamaterial with a periodic microstructure the optical emission and photoluminescence of an embedded quantum dot can be significantly changed; see Ref. [56] and other references cited therein. This occurs if the relevant frequency is in the vicinity of an EM resonance of the metamaterial, due to the great enhancement of the local electric field. Application of an external magnetic field $\mathbf{B}_0$ will presumably make those changes strongly dependent on the direction of $\mathbf{B}_0$ and on the polarization.

Effects similar to those described in this article are expected to appear for a periodically perforated metal film even if the holes are not perpendicular to the film plane. Further calculations are needed in order to show this in detail.

Some other recent achievements in nanoplasmonics and metamaterials [57] could also be changed by application of a strong static magnetic field $\mathbf{B}_0$.

It might also be interesting to consider the case where, rather than forming a single two-dimensional crystal, graphene is made as a perforated thin film with a periodic micro-structure [58].

ACKNOWLEDGMENTS

Partial support for this research was provided by grants from the U.S.-Israel Binational Science Foundation, the Russia-Israel Science Foundation, and the Israel Science Foundation, by MAFAT, and by the KAMEA Fellowship Program of the Ministry of Absorption of the State of Israel.

APPENDIX A: EVALUATION OF $\mathcal{E}_x$, δ_x, $\mathcal{E}_z$, δ_z.

1. General case

The analytical form of the parameters $\mathcal{E}_x$, δ_x, $\mathcal{E}_z$, δ_z introduced in Eqs. (21) and (22) can be found directly from

the following equations:

$$\mathcal{E}_x^2 = \left(\cos^2\frac{\phi'}{2} + \sinh^2\frac{\phi''}{2}\right) + \frac{\Delta'^2+\Delta''^2}{\sqrt{a^2+b^2}}\left(\sin^2\frac{\phi'}{2} + \sinh^2\frac{\phi''}{2}\right) + \frac{\sqrt{a+\sqrt{a^2+b^2}}}{\sqrt{2}\sqrt{a^2+b^2}}\left[(\Delta'\sinh\phi'' + \Delta''\sin\phi') + \frac{b}{a+\sqrt{a^2+b^2}}(\Delta''\sinh\phi'' - \Delta'\sin\phi')\right], \tag{A1}$$

$$\tan\delta_x = \frac{-\tan\frac{\phi'}{2}\tanh\frac{\phi''}{2} + \frac{\sqrt{a+\sqrt{a^2+b^2}}}{\sqrt{2}\sqrt{a^2+b^2}}\left[\left(\Delta''\tanh\frac{\phi''}{2} - \Delta'\tan\frac{\phi'}{2}\right) - \frac{b\left(\Delta'\tanh\frac{\phi''}{2} + \Delta''\tan\frac{\phi'}{2}\right)}{(a+\sqrt{a^2+b^2})}\right]}{1 + \frac{\sqrt{a+\sqrt{a^2+b^2}}}{\sqrt{2}\sqrt{a^2+b^2}}\left[\left(\Delta'\tanh\frac{\phi''}{2} + \Delta''\tan\frac{\phi'}{2}\right) + \frac{b\left(\Delta''\tanh\frac{\phi''}{2} - \Delta'\tan\frac{\phi'}{2}\right)}{(a+\sqrt{a^2+b^2})}\right]}, \tag{A2}$$

$$\mathcal{E}_z^2 = 4\frac{\eta'^2+\eta''^2}{\sqrt{a^2+b^2}}\left(\sin^2\frac{\phi'}{2} + \sinh^2\frac{\phi''}{2}\right), \tag{A3}$$

$$\tan\delta_z = -\frac{\left(1+\frac{\eta''}{\eta'}\frac{b}{a+\sqrt{a^2+b^2}}\right)\tan\frac{\phi'}{2} - \left(\frac{\eta''}{\eta'} - \frac{b}{a+\sqrt{a^2+b^2}}\right)\tanh\frac{\phi''}{2}}{\left(\frac{\eta''}{\eta'} - \frac{b}{a+\sqrt{a^2+b^2}}\right)\tan\frac{\phi'}{2} + \left(1+\frac{\eta''}{\eta'}\frac{b}{a+\sqrt{a^2+b^2}}\right)\tanh\frac{\phi''}{2}}. \tag{A4}$$

Here we have defined $\Delta^2 + 4\chi\eta^2 \equiv a + ib$, i.e.,

$$a \equiv \Delta'^2 - \Delta''^2 + 4\chi(\eta'^2 - \eta''^2), \tag{A5}$$

$$b \equiv 2(\Delta'\Delta'' + 4\chi\eta'\eta''). \tag{A6}$$

We also have taken into account that η, Δ, ϕ, etc., are complex parameters ($\eta = \eta' + i\eta''$, $\Delta = \Delta' + i\Delta''$, $\phi = \phi' + i\phi''$, etc.) and therefore $\sin(\frac{\phi'}{2} + i\frac{\phi''}{2}) = \sin\frac{\phi'}{2}\cosh\frac{\phi''}{2} + i\cos\frac{\phi'}{2}\sinh\frac{\phi''}{2}$, $\cos(\frac{\phi'}{2} + i\frac{\phi''}{2}) = \cos\frac{\phi'}{2}\cosh\frac{\phi''}{2} - i\sin\frac{\phi'}{2}\sinh\frac{\phi''}{2}$.

2. Faraday configuration

In Faraday configuration $\chi = -1$, $\Delta = \Delta' + i\Delta'' = 0$. From this follows that $\sqrt{a^2+b^2} = 4(\eta'^2+\eta''^2)$, $a + \sqrt{a^2+b^2} = 8\eta''^2$, $\frac{\eta''}{\eta'} - \frac{b}{a+\sqrt{a^2+b^2}} = \frac{\eta''^2+\eta'^2}{\eta'\eta''}$, and $1 + \frac{\eta''}{\eta'}\frac{b}{a+\sqrt{a^2+b^2}} = 0$. Equations (A1)–(A4) then simplify drastically:

$$\mathcal{E}_x^2 = \cos^2\frac{\phi'}{2} + \sinh^2\frac{\phi''}{2}, \tag{A7}$$

$$\tan\delta_x = -\tanh\frac{\phi''}{2}\tan\frac{\phi'}{2}, \tag{A8}$$

$$\mathcal{E}_z^2 = \sin^2\frac{\phi'}{2} + \sinh^2\frac{\phi''}{2}, \tag{A9}$$

$$\tan\delta_z = \tanh\frac{\phi''}{2}/\tan\frac{\phi'}{2}. \tag{A10}$$

After substituting Eqs. (A7)–(A10) into Eqs. (23) and (24) we get the well-known expressions for the Faraday rotation and ellipticity [37–41,59]:

$$\beta = \tfrac{1}{2}\phi', \tag{A11}$$

$$\sin 2\kappa = \tanh\phi'', \tag{A12}$$

where $\phi = \phi' + i\phi''$ is given by Eq. (20). This is in agreement with formulas presented in Refs. [39,40].

APPENDIX B: ELLIPSE OF POLARIZATION AND STOKES PARAMETERS

It is known that [60] the ellipse of polarization can be described in two ways: in arbitrary axes x, z or in the ellipse axes ξ, η (see Fig. 8). In the first case we use ratio of the amplitudes $|E_x|$ and $|E_z|$ [$\psi = \arctan(|E_x|/|E_z|)$] and phase

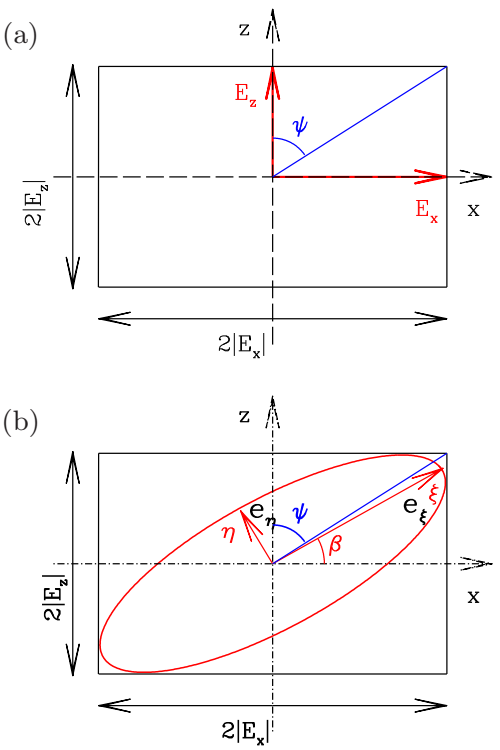

FIG. 8. (Color online) Ellipse of polarization. (a) Input; (b) output.

shift $\delta = \delta_x - \delta_z$. In the second case we use ratio of the minor to major axes e_η to e_ξ [i.e., ellipticity $\kappa = \pm \arctan(e_\eta/e_\xi)$] and the angle β of the major axis of the ellipse with respect to the x axis. Between these two pairs ψ, δ, and κ, β there exist several useful trigonometric relations. For example [60],

$$\tan 2\beta = -\tan 2\psi \cos\delta, \tag{B1}$$

$$\sin 2\kappa = \sin 2\psi \sin\delta. \tag{B2}$$

Since $\tan 2\psi$ can be expressed through $\tan\psi$, we can rewrite Eq. (B1) as follows: $\tan 2\beta = -2[\tan\psi/(1-\tan^2\psi)]\cos\delta$. Similarly, we can use the equality $\sin 2\psi = 2\sin\psi\cos\psi/(\cos^2\psi + \sin^2\psi) = 2\tan\psi/(1+\tan^2\psi)$.

The rotation angle β and the ellipticity κ can be also found from expressions

$$\beta = \frac{1}{2}\arctan\left(\frac{S_2}{S_1}\right), \quad 0 \leqslant \beta \leqslant \pi, \tag{B3}$$

$$\kappa = \frac{1}{2}\arcsin\left(\frac{S_3}{S_0}\right), \quad -\frac{\pi}{4} \leqslant \kappa \leqslant \frac{\pi}{4}, \tag{B4}$$

where S_0, S_1, S_2, S_3 are the Stokes parameters [42,61,62]:

$$S_0 = E_{0x}^2 + E_{0z}^2, \tag{B5}$$

$$S_1 = E_{0x}^2 - E_{0z}^2, \tag{B6}$$

$$S_2 = 2E_{0x}E_{0z}\cos\delta, \tag{B7}$$

$$S_3 = 2E_{0x}E_{0z}\sin\delta. \tag{B8}$$

[1] D. J. Bergman and Y. M. Strelniker, Phys. Rev. B **49**, 16256 (1994).
[2] D. J. Bergman and Y. M. Strelniker, Phys. Rev. B **86**, 024414 (2012), and references therein.
[3] D. J. Bergman and Y. M. Strelniker, Phys. Rev. Lett. **80**, 857 (1998).
[4] Y. M. Strelniker and D. J. Bergman, Phys. Rev. B **59**, R12763 (1999).
[5] M. Tornow, D. Weiss, K. v. Klitzing, K. Eberl, D. J. Bergman, and Y. M. Strelniker, Phys. Rev. Lett. **77**, 147 (1996).
[6] G. J. Strijkers, F. Y. Yang, D. H. Reich, C. L. Chien, P. C. Searson, Y. M. Strelniker, and D. J. Bergman, IEEE Trans. Magn. **37**, 2067 (2001).
[7] A. P. Vinogradov, A. V. Dorofeenko, A. M. Merzlikin, Y. M. Strelniker, A. A. Lisyansky, A. B. Granovsky, and D. J. Bergman, in *Magnetophotonics: From Theory to Applications*, edited by M. Inoue, M. Levy, and A. Baryshev (Springer, Berlin, 2013).
[8] V. I. Safarov, V. A. Kosobukin, C. Hermann, G. Lampel, J. Peretti, and C. Marliere, Phys. Rev. Lett. **73**, 3584 (1994).
[9] T. W. Ebbesen, H. J. Lezec, H. F. Ghaemi, T. Thio, and P. A. Wolff, Nature (London) **391**, 667 (1998); W. L. Barnes, A. Dereux, and T. W. Ebbesen, *ibid.* **424**, 824 (2003); C. Genet and T. W. Ebbesen, *ibid.* **445**, 39 (2007), and references therein.
[10] G. Dresselhaus, A. F. Kip, and C. Kittel, Phys. Rev. **98**, 368 (1955).
[11] Y. M. Strelniker and D. J. Bergman, Phys. Rev. B **77**, 205113 (2008).
[12] B. Sepulveda, L. A. Lechuga, and G. Armelles, J. Lightwave Technol. **24**, 945 (2006).
[13] N. Ou, J. H. Shyu, J. C. Wu, and T. H. Wu, IEEE Trans. Magn. **45**, 4027 (2009).
[14] V. V. Temnov, G. Armelles, U. Woggon, D. Guzatov, A. Cebollada, A. Garcia-Martin, J.-M. Garcia-Martin, T. Thomay, A. Leitenstorfer, and R. Bratschitsch, Nat. Photon. **4**, 107 (2010).
[15] G. Wurtz, W. Hendren, R. Pollard, R. Atkinson, L. L. Guyader, A. Kirilyuk, T. Rasing, I. I. Smolyaninov, and A. V. Zayats, New J. Phys. **10**, 105012 (2008).
[16] V. I. Belotelov, L. L. Doskolovich, and A. K. Zvezdin, Phys. Rev. Lett. **98**, 077401 (2007).
[17] A. B. Khanikaev, A. V. Baryshev, A. A. Fedyanin, A. B. Granovsky, and M. Inoe, Opt. Express **15**, 6612 (2007).
[18] A. Battula, S. Chen, Y. Lu, R. J. Knize, and K. Reinhardt, Opt. Lett. **32**, 2692 (2007).
[19] L. E. Helseth, Phys. Rev. B **72**, 033409 (2005).
[20] R. Zhou, H. Li, B. Zhou, L. Wu, X. Liu, and Y. Gao, Solid State Commun. **149**, 657 (2009).
[21] J. H. Kang, Q. H. Park, and D. S. Kim, J. Korean Phys. Soc. **55**, 1295 (2009).
[22] J. G. Han, A. Lakhtakia, Z. Tian, X. Lu, and W. Zhang, Opt. Lett. **34**, 1465 (2009).
[23] D. M. Newman, M. L. Wears, and R. J. Matelon, Europhys. Lett. **68**, 692 (2004).
[24] A. Garcia-Martin, G. Armelles, and S. Pereira, Phys. Rev. B **71**, 205116 (2005).
[25] G. Armelles, J. B. Gonzales-Diaz, A. Garcia-Martin, J. M. Garcia-Martin, A. Cebollada, M. U. Gonzales, S. Acimovich, J. Cesario, R. Quidant, and G. Badenes, Opt. Express **16**, 16104 (2008); J. B. Gonzalez-Diaz, A. Garcia-Martin, and G. Armelles Reig, Nanoscale Res. Lett. **6**, 408 (2011); J. F. Torrado, J. B. Gonzalez-Diaz, M. U. Gonzalez, A. Garcia-Martin, and G. Armelles, Opt. Express **18**, 15635 (2010).
[26] B. Sepulveda, J. B. Gonzalez-Diaz, A. Garcia-Martin, L. M. Lechuga, and G. Armelles, Phys. Rev. Lett. **104**, 147401 (2010).
[27] J. B. Gonzalez-Diaz, B. Sepulveda, A. Garcia-Martin, and G. Armelles, Appl. Phys. Lett. **97**, 043114 (2010).
[28] E. Melander, E. Ostman, J. Keller, J. Schmidt, E. T. Papaioannou, V. Kapaklis, U. B. Arnalds, B. Caballero, A. Garcia-Martin, J. C. Cuevas, and B. Hjorvarsson, Appl. Phys. Lett. **101**, 063107 (2012).
[29] L. Halagacka, M. Vanwolleghem, K. Postava, B. Dagens, and J. Pistora, Opt. Express **21**, 21741 (2013).
[30] V. L. Krutyanskiy, I. A. Kolmychek, E. A. Gan'shina, T. V. Murzina, P. Evans, R. Pollard, A. A. Stashkevich, G. A. Wurtz, and A. V. Zayats, Phys. Rev. B **87**, 035116 (2013).
[31] W. J. Tabor and F. S. Chen, J. Appl. Phys. **40**, 2760 (1969).
[32] Y. M. Strelniker, D. Stroud, and A. O. Voznesenskaya, Eur. Phys. J. B **52**, 1 (2006).
[33] Y. M. Strelniker, D. Stroud, and A. O. Voznesenskaya, J. Appl. Phys. **99**, 08H702 (2006).

[34] Y. Fleger, M. Rosenbluh, Y. M. Strelniker, D. J. Bergman, and A. N. Lagarkov, Eur. Phys. J. B **81**, 85 (2011).
[35] S. D. Smith, in *Light and Matter, Ia, Encyclopedia of Physics*, edited by L. Genzel (Springer-Verlag, Berlin-Heidelberg, 1967), pp. 234–318.
[36] M. S. Kushwaha and P. Halevi, Phys. Rev. B **35**, 3879 (1987).
[37] N. Saleh and S. Zukotynski, Phys. Stat. Sol. **37**, 879 (1970).
[38] R. Stevenson, Can. J. Phys. **38**, 941 (1960).
[39] P. N. Argyres, Phys. Rev. **97**, 334 (1955).
[40] E. D. Palik and J. K. Furdyna, Rep. Prog. Phys. **33**, 1193 (1970).
[41] F. Abeles, in *Optical Properties of Metals*, edited by F. Abeles (North-Holland, Amsterdam, 1972), pp. 93–162; J. G. Mavroides, *ibid*., pp. 351–528.
[42] S. Pakdel and M. F. Miri, Phys. Rev. B **86**, 235445 (2012).
[43] Y. M. Strelniker and D. J. Bergman, Phys. Rev. B **67**, 184416 (2003).
[44] Y. M. Strelniker and D. J. Bergman, J. Magn. Magn. Mater. **321**, 814 (2009).
[45] D. J. Bergman and Y. M. Strelniker, Phys. Rev. B **82**, 174422 (2010).
[46] Y. M. Strelniker and D. J. Bergman, Phys. Rev. B **50**, 14001 (1994).
[47] D. J. Bergman, in *Les Méthodes de l'Homogénéisation: Théorie et Applications en Physiques*, edited by R. Dautray (Editions Eyrolles, Paris, 1985), p. 1128.
[48] D. Stroud, Phys. Rev. B **12**, 3368 (1975).
[49] D. J. Bergman and K. J. Dunn, Phys. Rev. B **45**, 13262 (1992).
[50] D. J. Bergman and Y. M. Strelniker, Phys. Rev. B **51**, 13845 (1995).
[51] Y. M. Strelniker and D. J. Bergman, Phys. Rev. B **53**, 11051 (1996).
[52] D. J. Bergman, X. T. Li, and Y. M. Strelniker, Phys. Rev. B **71**, 035120 (2005).
[53] R. E. Sherriff and R. P. Devaty, Phys. Rev. B **41**, 1340 (1990).
[54] R. E. Sherriff and R. P. Devaty, Phys. Rev. B **48**, 1525 (1993).
[55] L. M. Claessen, A. G. M. Jansen, and P. Wyder, Phys. Rev. B **33**, 7947 (1986).
[56] M. R. Singh, J. D. Cox, and M. Brzozowski, J. Phys. D: Appl. Phys. **47**, 085101 (2014).
[57] S. A. Maier, *Plasmonics: Fundamentals and Applications*, 2nd ed. (Springer, New York, 2007).
[58] In a recent paper [I. Crasse, J. Levallois, A. L. Walter, M. Ostler, A. Bostwick, I. Rotenberg, T. Seyller, D. van der Marel, and A. B. Kuzmenko, Nat. Phys. **7**, 48 (2011)], it was discovered that graphene exhibits a huge Faraday effect: 6° rotation of linear polarization by just one layer of graphene and $|\mathbf{B}_0| = 7$ T applied perpendicular. No anisotropy was reported. It might be interesting to consider what will happen if the $\mathbf{B}_0$ field is applied parallel to the graphene layer made as a perforated thin film with a periodic microstructure.
[59] L. D. Landau, E. M. Lifshitz, and L. P. Pitaevskii, *Electrodynamics of Continuous Media* (Pergamon Press, Oxford, 1984).
[60] M. Born and E. Wolf, *Principles of Optics: Electromagnetic Theory of Propagation, Interference and Diffraction of Light* (Cambridge University Press, Cambridge, UK, 2005).
[61] M. I. Mishchenko, J. W. Hovenier, and L. D. Travis, eds., *Light Scattering by Nonspherical Particles: Theory, Measurements, and Applications* (Academic Press, San Diego, 2000).
[62] E. Collett, *Field Guide to Polarization* (SPIE Press, Bellingham, WA, 2005).